frontiers in Physics

REVIEW
published: 15 April 2021
doi: 10.3389/fphy.2021.641341

# High-Resolution Optical Imaging and Sensing Using Quantum Emitters in Hexagonal Boron-Nitride

*Carlo Bradac* *

*Department of Physics and Astronomy, Trent University, Peterborough, ON, Canada*

Super-resolution microscopy has allowed optical imaging to reach resolutions well beyond the limit imposed by the diffraction of light. The advancement of super-resolution techniques is often an application-driven endeavor. However, progress in material science plays a central role too, as it allows for the synthesis and engineering of nanomaterials with the unique chemical and physical properties required to realize super-resolution imaging strategies. This aspect is the focus of this review. We show that quantum emitters in two-dimensional hexagonal boron nitride are proving to be excellent candidate systems for the realization of advanced high-resolution imaging techniques, and spin-based quantum sensing applications.

**Keywords: hexagonal boron-nitride, quantum emitters, super-resolution microscopy, quantum sensing, van der waals materials**

OPEN ACCESS

***Edited by:***
*Qiuqiang Zhan,*
*South China Normal University, China*

***Reviewed by:***
*Chaohao Chen,*
*University of Technology Sydney, Australia*
*Nirmal Mazumder,*
*Manipal Academy of Higher Education, India*
*Yan-Kai Tzeng,*
*Stanford University, United States*

***Correspondence:**
*Carlo Bradac*
*carlobradac@trentu.ca*

***Specialty section:***
*This article was submitted to Optics and Photonics, a section of the journal Frontiers in Physics*

***Received:*** *16 December 2020*
***Accepted:*** *19 February 2021*
***Published:*** *15 April 2021*

***Citation:***
*Bradac C (2021) High-Resolution Optical Imaging and Sensing Using Quantum Emitters in Hexagonal Boron-Nitride. Front. Phys. 9:641341. doi: 10.3389/fphy.2021.641341*

## INTRODUCTION

### Super-Resolution Microscopy

Super-resolution microscopy (SRM) has expanded optical imaging to resolutions well beyond the diffraction limit of light. While traditional microscopy techniques can resolve lateral spot sizes ~200–300 nm (and ~500–700 nm, axially), super-resolution fluorescence microscopy can achieve resolutions of the order of ~20–50 nm, and in some cases <10 nm [1–3]. The key of SRM is to render the fluorophores within the same diffraction region transiently discernible from one another for a short period of time. This is achieved through several strategies (briefly summarized below) that exploit the specific optical properties of photoluminescent materials, such as the non-linearity or stochastic nature of their emission.

### Resolft

In reversible saturable/switchable optical linear fluorescence transitions (RESOLFT) microscopy, the super-resolved detection of individual emitters is achieved through non-linear optical excitation and emission schemes. RESOLFT microscopy generalizes the principles of techniques such as stimulated emission depletion (STED) and ground state depletion (GSD) microscopy [4, 5]. These usually involve point-scanning strategies where the laser excitation and photoluminescence collection are designed ad hoc. A standard approach is to co-excite the sample with a torus-shaped beam overlapped to a confocal one to selectively induce "off" and "on" states in the fluorophores, and separate them in time/space as the beam is scanned across the sample. RESOLFT approaches can routinely achieve lateral resolutions of ~40–80 nm.

## Structured Illumination

In structured illumination microscopy (SIM) the sample is illuminated by high spatial-frequency patterns with a specific profile e.g., parallel lines [6]. Fluorophores are resolved beyond the diffraction limit as their emission combined with the patterned illumination generates large and detectable interference patterns. The incident pattern is applied in different orientations, and the super-resolution image is mathematically deconvolved from the interference signal. SIM methods can reach lateral and axial resolutions of ~125 nm and 350 nm, respectively. Higher lateral resolutions of ~50 nm can be achieved combining SIM with RESOLFT strategies, as for the case of nonlinear SIM [7] and instant SIM [8].

## Stochastic Methods

Rather than through point-scanning or structured excitation, single-molecule localization microscopy (SMLM) achieves sub-diffraction resolution via wide-field illumination. The emission of the fluorophores is photo-controlled as these are switched "on" and "off" by the laser. This is the case, for instance, for stochastic optical reconstruction microscopy (STORM) [9] and photoactivated localization microscopy (PALM) [10, 11]. Different fluorophores within the (wide-field) excitation area are detected individually as their photo-blinking and/or -bleaching behavior render them optically active and inactive at different (random) times. Stochastic, state-switching detection is also the working principle of points accumulation for imaging in nanoscale topography (PAINT) [12]. PAINT exploits single fluorophores becoming optically "bright" as they (reversibly) bind to a target structure, which in turns makes them individually distinguishable from the "dark", unbound ones. Stochastic methods can generally achieve lateral resolutions of ~20–25 nm with advanced setups reaching the ~5 nm limit.

## Off-State Microscopy

A particularly powerful SRM approach is minimal photon flux microscopy (MINFLUX) [3, 13]. The method can operate both with scanning beam and standing wave microscopy arrangements. It relies on detecting the position of single fluorophores at the deep intensity minimum of e.g., a torus-shaped excitation spot, as this is sequentially moved in space. The location of the emitter is inferred using a statistical maximum likelihood strategy that estimates the exact position based on where the fluorescence intensity is ~zero (i.e., where the emitter is minimally excited at the center of the torus beam). MINFLUX microscopy can achieve lateral resolutions of ~1–3 nm. Variants of MINFLUX include multiple off-state transitions for nanoscopy [14] and MINFIELD [15], which are designed to improve resolution, signal contrast and/or temporal sampling while reducing the light dose to the sample.

## The Role of Material Science in SRM

Super resolution microscopy is an active field of research whose steady objective is to both develop new SRM approaches and design strategies to improve existing ones. Notably, this is not a mere application-driven endeavor. On one hand super-resolution microscopy has certainly being advanced as an indispensable characterization tool; for example in biology for monitoring cellular and subcellular processes [1], or in material science for studying complex materials [16]. On the other hand however, SRM has certainly been advanced by the progress made in material science and in the synthesis of nanomaterials with the unique chemical and physical properties required to realize super-resolution imaging strategies. This second aspect is the focus of this review. The goal is to present and discuss recent developments in high resolution imaging and sensing applications based on a specific two-dimensional material: hexagonal boron-nitride (hBN). We show that this material possesses distinctive physical and spin-optical properties that make it a desirable system for advanced realizations requiring the measurement of objects and quantities at the nanoscale.

This review is organized as per the following. The first part focuses on the hBN material and its properties. Emphasis is put on those most relevant for high resolution (bio)imaging and (bio) sensing such as the material's optical properties, the synthesis of hBN nanostructures as well as their toxicity, surface chemistry and functionalization. The second part discusses a selection of the most recent fundamental and practical realizations in super-resolution microscopy and spin sensing based on quantum emitters in hBN.

# HEXAGONAL BORON-NITRIDE

Hexagonal boron-nitride (hBN) is a two-dimensional (2D) van der Waals (vdW) material. Two-dimensional materials which also include materials of the graphene family, 2D chalcogenides and 2D oxides are rapidly becoming one of the most studied subject in condensed matter physics [17]. Their low dimensionality confers them unique properties. For instance, they can be used to engineer heterostructure and hybrid devices consisting of ordered stacks of atom-thin layers, with designer properties [17, 18]. They are being widely utilized to explore characteristic physical phenomena [17, 19, 20] such as Moiré patterns [21], high-temperature quantum spin Hall effect [22] and interlayer excitons with valley-/spin-contrasting degrees of freedom [23–27]. Besides fundamental studies, vdW heterostructures are also largely investigated for technological realizations e.g., in electronic, opto-electronic and nanophotonic devices such as lasers [28], diodes [29], transistors [30–33], sensors [34, 35], photodetectors [36–38] and amplifiers [39].

Here, we focus specifically on hexagonal boron-nitride and its recent developments as a desirable material for high-resolution imaging and sensing. The material's properties are therefore presented with attention to the main key features required for ideal (bio)probes: 1) bright and photo-stable or controllable fluorescence, 2) small size (<10 nm), 3) non-toxicity, 4) room-temperature operation, water solubility and ability to withstand pH variability, 5) controllable chemistry and high binding-specificity.

## Crystalline Structure

Two-dimensional hexagonal boron-nitride is a van der Waals material with a graphite-like crystalline structure where boron

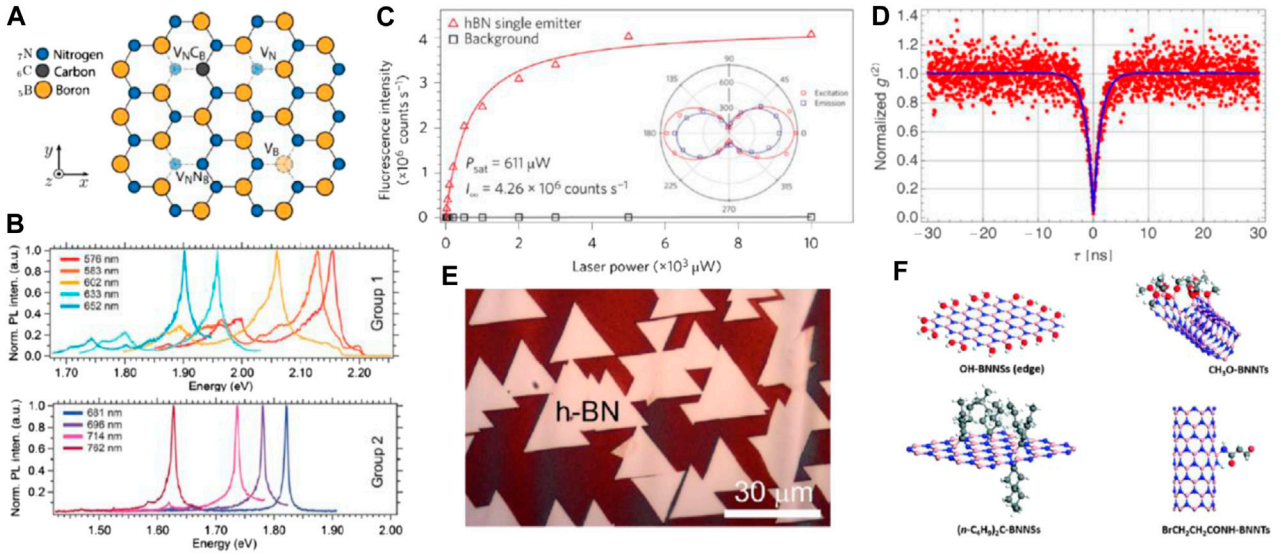


**FIGURE 1 |** Properties of hexagonal boron-nitride. **(A)** Crystalline structure of hBN and point defects consisting of (complexes of) vacancies and foreign atoms. **(B)** Multicolor photoluminescence from point defects in hBN. **(C)** Photoluminescence saturation curve from a single hBN defect (maximum emission rate $4.26 \times 10^6$ counts/s). Inset: excitation (red, circles) and emission (blue, squares) polarization curves from a single hBN defect. **(D)** Second-order autocorrelation measurement $g^{(2)}(\tau = 0) = 0.033\,(47)$ of a single hBN defect, indicating the quantum (single-photon emission) nature of the emitter (conventionally attributed for $g^{(2)}(0) < 0.5$). **(E)** Optical image of hBN grown for 10 min on copper foil by atmospheric pressure chemical vapor deposition (APCVD). **(F)** Schematics of a selection of functionalized boron-nitride nanosheets and nanotubes. Figures adapted and reprinted with permission: **(A)** [53] Copyright American Chemical Society 2018; **(B)** [54] Copyright American Chemical Society 2016; **(C)** [52] Copyright Springer Nature 2015; **(D)** [60] Copyright American Chemical Society 2018; **(E)** [140] Copyright WILEY-VCH Verlag GmbH & Co. KGaA, Weinheim 2019; **(F)** [111] Royal Society of Chemistry 2016.

and nitrogen atoms are organized in atom-thin layers stacked over one another (**Figure 1A**). Within each layer, B and N atoms are bound in a honeycomb hexagonal lattice (lattice constant 2.504 Å). The B–N bonds are *sp* [2]-hybridized, partially covalent and partially ionic, with the electron pairs more confined to the N atoms due to their high electronegativity.

The different atomic layers are instead connected (layer spacing 3.30–3.33 Å) mainly via weaker van der Waals forces [40]. This structure makes hBN a versatile material that can be produced using different methods and in a variety of nanostructures. The material has a large energy bandgap of ~5–6 eV [41], which is the basis of some of its optical properties (Note that values of the bandgap have been reported in the wider range 3.6–7.1 eV [42], with the variability depending on hBN being mono- or multi-layered and on the stacking arrangement of its layers [43, 44]).

## Optical Properties

Hexagonal boron-nitride exhibits optical properties which are the foundations of several photoluminescence-based imaging and sensing applications. Being a wide-bandgap material, pristine hBN is nominally transparent in the visible spectral range (~390–700 nm). It displays absorption and emission in the deep ultraviolet (~210–220 nm) due to generation and recombination of free (~215 nm) and bound excitons (~227 nm) [45, 46].

However, hBN generally hosts various type of crystalline defects: dislocations, grain boundaries, edges, vacancies and interstitial atoms [47–53]. Amongst these, atom-like defects consisting of complexes of vacancies and/or foreign atoms are of particular interest, as they give rise to characteristic photoluminescence emission in the visible and near infrared spectral range (**Figures 1A,B**) [54, 55].

Besides a few exceptions [56–58], the exact chemical composition and structure of these defects are still unknown. Yet, these so-called color centers are widely utilized in both fundamental and practical realizations as they display properties that are ideal for photoluminescence-based applications (**Figures 1A–D**). These include bright, polarized [52], multi-wavelength [54], single-photon (quantum) emission [52], as well as chemical stability [59], high photon purity [58, 60, 61], large stark-shift wavelength tuning [62, 63], non-linear photo-physics compatible to super-resolution imaging [64, 65], and addressable spin-dependent photo-emission [56].

Note also that due to the 2D nature of the host hBN material, the photon extraction efficiency from these atom-like emitters is comparatively high (~$10^6$ counts/s at saturation)—as phenomena like Fresnel and total internal reflection, scattering and re-absorption are negligible [60]. This is ideal for photoluminescence-based applications as high collection efficiencies translate into high signal-to-noise ratio and thus better signal and/or temporal resolution.

## Synthesis and Nanostructures

One of the key factors for practical high-resolution imaging and sensing applications is the ability to readily fabricate fluorescent nanoprobes. In this regard, hBN is an extremely versatile material as there are several methods available to synthesize 2D BN

nanostructures, either via bottom-up or top-down methods. Bottom-up techniques include synthesis by chemical vapor deposition (**Figure 1E**) [66–68], segregation [69] and by solid-state [70] or substitution reaction [71]. Top-down approaches include mechanical [72–75] or chemical exfoliation [76–79], as well as high-energy electron irradiation [80, 81].

Boron-nitride nanomaterials (BNNs) include zero-dimensional (0D) fullerenes and nanoparticles, one-dimensional (1D) nanotubes and nanoribbons, two-dimensional (2D) nanosheets and three-dimensional (3D) nanoporous BN. There are extensive reviews dedicated to the fabrication of BNNs [82, 83], here we briefly summarize the methods developed to fabricate fluorescent nanoparticle-like (0D) objects, which are used in some of the SRM applications described below. Common nanofabrication approaches include the breaking down of large hBN microscopic crystals into nanosized hBN particles e.g., via ball-milling [84] or acoustic cavitation [85, 86]. These methods can usually achieve high yields of hBN nanoparticles, but their size is relatively large (~tens or ~ hundreds of nm), especially for applications in bio-imaging and nanoscale sensing. Recently however, high yields of hBN nanoparticles less than 10 nm in size have been achieved via cryogenic-induced cracking of hBN [87, 88] and by hydrothermal synthesis [89]. It should be noted that at this size the photostability of the emitters can be compromised—giving rise to photo-blinking and -bleaching—due to interaction with surface states and fluctuations in the local electric field. These are associated, for instance, with dangling bonds, other point-defects, or trapped charges, whose effect becomes more prominent as the particle size reduces [90–93]. These effects can partially be reduced with surface passivation strategies [94–97], but must be taken into account for assessing the reliability of the probes. In some cases however, they are central to achieve super-resolution imaging and are therefore a desirable feature.

## Non-toxicity

Boron-nitride is considered a suitable material for biological and medical applications. Boron-nitride nanomaterials (BNNs) possess good biocompatibility [98–101] and high chemical and mechanical stability [102, 103]. BNNs have been found not to inhibit cell growth or induce apostosis [104, 105] and they have been shown to be up-taken by cells [99, 106, 107]. In fact, they have been used in practical realizations including as drug and gene carriers [108] and in cancer treatment studies [109]. For completeness, it should be noted that time-, dose- and cell-dependent cytotoxicity of BNNs has been reported in a small number of studies [108, 110].

## Functionalization

The chemical functionalization of boron-nitride nanomaterials (BNNs) is challenging as, in general, the network of B and N atom connected by *sp* [2]-hybridized bonds is highly stable and chemically inert. Nevertheless, several functionalization strategies have been proposed and realized, albeit with low overall yields (**Figure 1F**) [111]. Note that both N and B can be utilized for functionalization whenever they are at an edge or at a lattice defect, where they give rise to dangling bonds. Conversely, reactions on the basal plane require opening of the B–N bonds. Both B and N must be terminated either by multiple functional groups (to balance the overall charge) or via a bridging bond. The B–N bond is partly covalent and partly ionic, which makes the nitrogen and boron atoms partially negatively and positively charged, respectively, due to their different electronegativity. As a result, B tends to bind to nucleophile (electron-donating) groups while N to electrophile (electron-accepting) ones. The list of functional groups successfully conjugated to BN nanomaterials include hydroxyl (–OH), amino ($–NH_2$), ether (–OR), amine (–NHR), arcyl (–COR), alkyl (–R), and halogen (–X) groups. The relevant functionalization methods can be found in dedicated reviews [111–114] and are summarized here, briefly.

*Hydroxyl groups.* Hydroxyl groups (–OH) are amongst the most fundamental functionalization groups for BNNs both for direct applications (matrix filling and bio-applications) and as base for more complex conjugations. The functionalization of BNNs—in particular BN nanotubes and nanosheets—with–OH groups is generally achieved via covalent bonding to B sites and has been realized through a series of alternative approaches including plasma treatment, hydrothermal reactions with NaOH, NaOH-assisted ball-milling, and reactions with $H_2O$ at a high temperature, or using reagents that can generate OH radicals [115–121].

*Amino and amine groups.* Analogously to hydroxyl (–OH) group, the electrophilic B centers can be functionalized with amino ($–NH_2$) and amine (–NHR) groups. This can be achieved for instance by plasma treatment, etched-assisted sonication and urea-assisted ball-milling [122–125].

*Alkoxy groups.* Alkoxy groups consisting of an alkyl group (carbon and hydrogen chain) bonded to an oxygen atom (–OR) can be functionalized directly onto BN surfaces e.g., by sonication in primary alcohols solvents [126]. Note that the–OR termination is advantageous for applications that require (alcoholysized) BN nanostructures to be readily dispersed in alcohol solvents.

*Alkyl groups.* Alkyl (–R) groups can attach to BN by forming B–C–N bridges or directly on B or N sites. This has been realized e.g., by carbene-assisted substitution and by reaction with a reductant solution and hexyl-containing compounds [127, 128].

*Other groups.* A whole suite of other groups has been successfully conjugated to BNNs. For instance, esterified (–OCOR), amidated (–NHCOR) and acylated (–COR) groups have been attached to BN nanostructures directly from their BN precursors or via their hydroxylated (OH-BN) and aminated ($NH_2$-BN) intermediates [116, 118, 124, 129–132]. Functionalization with hydrogen and fluorine, as well as other groups ($–CH_3$, –CHO, –CN, –OH, $–NH_2$, etc.), has been also largely investigated as these species can significantly affect the material properties such as the BNNs stability, bandgap energy and electronic properties [133–135].

It is important to note that the ability to readily functionalize BN nanostructures—e.g., for stability in physiological environments and for target-specific labelling of subcellular structures—is only one of the aspects that must be considered

**TABLE 1 |** Super-resolution imaging techniques based on hBN emitters.

| System | Method | Mechanism | Resolution |
|---|---|---|---|
| SPEs in hBN flakes 64 | RESOLFT, off-state microscopy | Non-linear excitation of SPEs with repumping from metastable state(s) | (63 ± 4) nm |
| SPEs ($V_B$) in hBN monolayers 141 | SMLM | Stochastic on/off photo-blinking between charge states ($V_B^0 \leftrightarrow V_B^-$) | 10.7 nm |
| SPEs in hBN nanoparticles (≥3 nm) 87 | SMLM | Stochastic on/off photo-blinking | <10 nm |
| SPEs in monolayer/bulk hBN 65 | SMLM | Stochastic on/off photo-blinking combined with spectral analysis | ~10 nm |
| SPEs ($V_B^-$) in multilayer hBN 142 | SMLM | Stochastic on/off photo-blinking due to protonation of SPEs ($V_B^- + H^+ \rightarrow V_BH$) | ~5–40 nm |

for super-resolution imaging and sensing. Another critical factor to take into account is determining whether the presence of functionalized groups on the surface of the BN nanostructures alters their optical properties, possibly hindering their suitability as super-resolution probes. When nanostructures are smaller than a few nanometers, surface effects become relevant and the fluorescence of the hosted emitter can undergo intensity fluctuations, spectral diffusion, photoluminescence intermittency ("blinking") or even cease all together. These effects are not unique to hBN but rather universal and are due to the presence of surface states (e.g., dangling bonds, point-defects, trapped charges and conjugated chemical species) which can drive the emitter in different charge states or generate random electric fields that destabilize the optical dipole moments of the emitters via spontaneous Stark shifts [93, 136, 137].

There are two main considerations to make in this regard. Firstly, these effects can be mitigated via specific surface passivation of the hBN nanoprobes. Suitable approaches are already available e.g., sol-gel coating via Stober reaction [138, 139]. Besides, establishing whether certain functionalization groups deteriorate the optical properties of the BN nanoprobes is both feasible and experimentally testable. Secondly, in some cases the photo-instability of the probes is a desirable—in fact, necessary—feature. It allows for super-resolution imaging schemes based on the stochastic intermittency of individual, and otherwise unresolvable, emitters between "on" and "off" states, over time.

## SUPER-RESOLUTION IMAGING WITH HBN

Standard, diffraction-limited microscopy using hexagonal boron-nitride nanomaterials (BNNs) is well established. Yet, super-resolution imaging has been realized only recently, thanks to the discovery and control of specific optical properties associated with quantum emitters in hBN (**Table 1**) [64, 141].

### Resolft

One of the first demonstration of super-resolution imaging in hBN was realized in 2018 [64]. The technique utilizes the non-linear behavior of a specific class of hBN single-photon emitters (SPEs). The exact nature and chemical structure of these hBN emitters is unknown—the emission is likely due to transition between energy states in the hBN bandgap associated to atom-like defects in the lattice. Regardless, the non-linear behavior is observed consistently for an entire family of them with zero-phonon line (ZPL) emission wavelengths >700 nm.

Upon excitation with a laser (at 675 nm or 708 nm in the study), the emitters produce a photoluminescence signal with a sharp ZPL (e.g., 785 nm). When co-excited with a second low-power (~30× less) laser at a shorter wavelength (532 nm), the emitters show a highly non-linear behavior characterized by an increase in photoluminescence (~2×) and lowering (~5×) of their saturation intensity. This non-linear behavior is attributed to the 532 nm laser repumping the system from a metastable "dark" state back to the excited "bright" state. The existence of photo-switchable dark/bright emission states is one of the main requirements for RESOLFT super-resolution microscopy. This unique photo-physical behavior can thus be harnessed to realize a variant of saturable, far-field, sub-diffraction fluorescence nanoscopy, which is what was done in the study.

The technique has two notable advantages. Hexagonal boron-nitride emitters are extremely robust against high-power illumination [143]. Whilst this is not a requirement for RESOLFT SRM, it is a desirable feature. For instance, both in STED and GSD the transition from the "bright" to the "dark" state is achieved by optical saturation—via stimulated emission depletion and ground-state depletion, respectively. This usually requires high excitation powers, which can lead to photo-bleaching of the emitters—a problem that has led to the development of off-state transitions nanoscopy methods. In addition, the issue of requiring high laser excitations for inducing saturation is further alleviated with this approach, as the second repumping laser effectively reduces the saturation intensity of the emitters. This is shown in the study where a negative-GSD-like scheme is utilized to assess the resolution of the technique (**Figure 2A**).

In the first experiment, a single torus beam (708 nm) is used as the excitation source. As the beam is scanned, the emitter is excited by a high–null–high intensity profile and produces a corresponding high–null–high emission pattern. In the confocal image, the emitter's location thus coincides with the center of the emission null (like in standard off-state transitions nanoscopy) and is readily extracted via mathematical deconvolution of the inverse image (**Figure 2A**, right). Sub-diffraction resolution is achieved as at higher excitation powers of the scanning torus beam, the high–null and null–high photoluminescence emission gradients become steeper. This effectively narrows the full width at half-maximum (FWHM) of the emission null according to the relation:

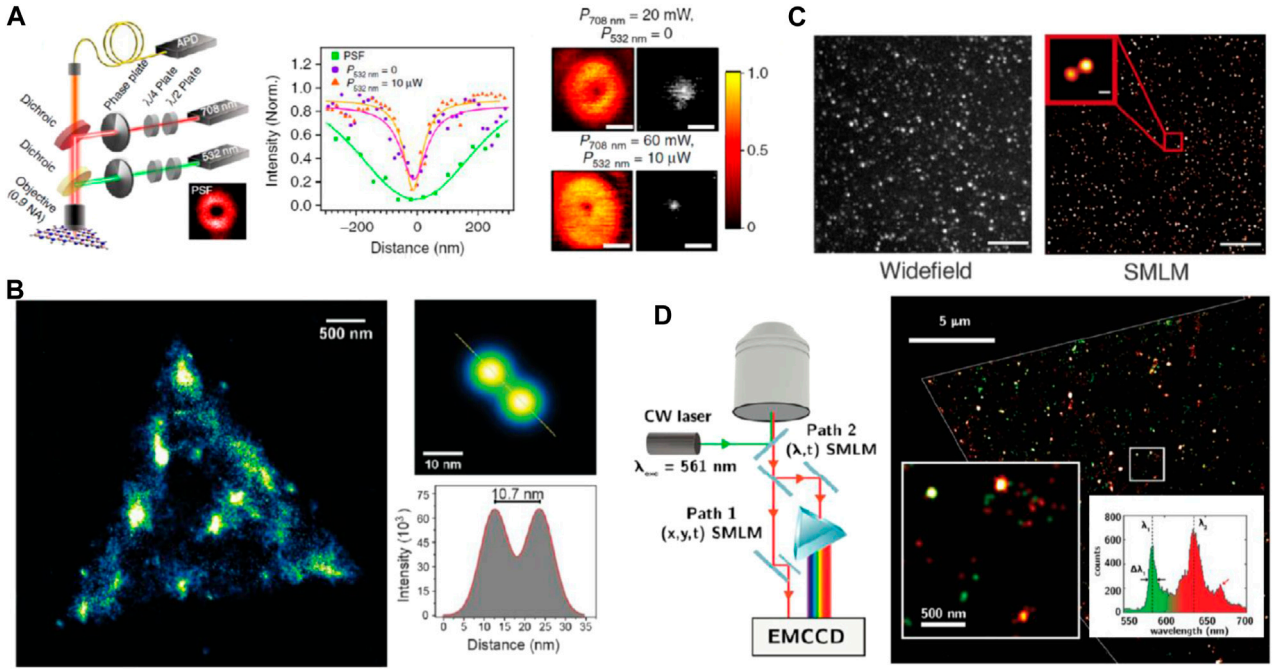


**FIGURE 2 |** RESOLFT and SMLM microscopy in hBN. **(A)** Super-resolution microscopy using dual torus-beam excitation. Left: schematics of the experiment. Center: point spread function of the confocal system (green), and resolutions obtained under 708 nm torus-beam laser excitation only (violet) and adding a second 532 nm torus-beam (orange). Right: the resolution increases upon increasing the intensity of both the 708 nm and the 532 nm lasers. **(B)** SMLM imaging of optically active defects in hBN reconstructed from an image sequence of 20,000 frames, display pixel size: 1 nm. With drift correction using fiducial markers, the method achieves a resolution of 10.7 nm **(C)** Widefield and SMLM reconstructed image (based on 6,000 frames) of an ensemble of hBN nanoparticles (average size (3.0 ± 0.7) nm), synthesized by cryo-exfoliation (scale bar: 5 µm). Inset: zoomed-in section showing two emitters in the super-resolved image (scale bar: 100 nm). **(D)** Multimodal SMLM. Left: schematics of the experiment showing dual spatial and spectral detection. Right: Spatial and spectral distribution of centers in a CVD-grown hBN flake. A dual spectral distribution is visible corresponding to green and red emitters with emission wavelength $\lambda_1$ and $\lambda_2$ (right inset). Figures adapted and reprinted with permission: **(A)** [64] Copyright Springer Nature 2018; **(B)** [141] Copyright American Chemical society 2018; **(C)** [87] Copyright American Chemical society 2019; **(D)** [65] Copyright American Chemical society 2019.

$$\Delta r \cong \lambda(\beta\pi n)^{-1}\sqrt{\varepsilon + \frac{I_s}{I_m}} \tag{1}$$

where $\Delta r$ is the resolution; $I_m$ is the maximum laser intensity in the periphery of the torus, and $\varepsilon I_m$ is the minimum (null) intensity in the center. The quantity $I_s$ is the saturation intensity, while $\lambda$ and $n$ are the wavelength and the refractive index, respectively. The parameter $\beta$ is the steepness of the point spread function which depends on the emitter's properties and on the periphery-to-minimum intensity gradient of the toroidal excitation beam.

**Equation 1** shows that the resolution $\Delta r$ improves ($\Delta r$ becomes smaller) when the ratio $I_s/I_m$ is minimized. Generally, in other RESOLFT approaches, this is done by increasing the excitation laser intensity $I_m$ well above $I_s$. This method, however, also allows to directly reduce $I_s$ via the re-pumping mechanism. This was demonstrated in a subsequent experiment of the study (**Figure 2A**, left and center panel), where a second torus beam (532 nm laser) was superimposed to the first one (708 nm laser). The addition of the 532 nm toroidal beam effectively reduces $I_s$ minimizing the ratio $I_s/I_m$, for any given intensity $I_m$ of the excitation torus at 708 nm. The highest resolution achieved using just the 708 nm excitation torus was (87 ± 10) nm, slightly worse than (63 ± 4) nm obtained with the two 708 nm and 532 nm torus beams overlapped. Both resolutions are far better than the ~460 nm value of the confocal setup used in the study.

As a final point, it should be noted that this variant of SRM developed using hBN emitters could be extended to other classes of fluorophores, provided that they possess an analogous behavior characterized by the ability of the system to be re-pumped from the ("dark") metastable state to the excited ("bright") state.

## Single-Molecule Localization Microscopy (SMLM)

Simultaneously to the approach described in §3.1, SRM was also realized in hBN monolayers using single-molecule localization microscopy [141]. The method exploits the on/off photo-switching behavior (blinking) of hBN emitters, which allows for their temporal—and thus spatial—separation, by capturing them when they are "bright/dark" alternately, one at a time (**Figure 2B**).

Note that the photo-stability of hBN emitters depends on their local environment as, e.g., electric field fluctuations and nearby trap states can induce phenomena such as spectral diffusion and

blinking [144, 145]. In the case of hBN, photo-blinking is often more prominent for small (<10 nm) and thin (~monolayer) nanoparticles/nanoflakes as the proximity to the surface increases the probability of local perturbations.

In the study, the sample consisted of a hBN monolayer. The material shows optically active emitters which are attributed to boron monovacancies $V_B$ (i.e., a missing B atom in the hBN lattice)—as deduced form transition electron microscopy (TEM) analysis. The blinking behavior of the emitters is attributed to photo-induced ionization and recombination between the neutral $V_B^0$ and negatively charged $V_B^-$ states. For SMLM to work, the sample must be spatially fixed with no drift over time. This can be achieved either through the use of a closed-loop feedback-controlled stage or, like in this study, through post processing alignment using fiducial markers. The spatial resolution achieved in the study is 10.7 nm (**Figure 2B**, right panels).

The approach has a few desirable features. It utilizes wide-field illumination and detection of large sample areas (~up to tens of μm) with fast acquisition (~ms) and minimum damage to the sample thanks to the low power density (~100 kW/m$^2$) of the excitation laser, compared to e.g., STED microscopy. It also allows for probing the chemical reactivity of the emitters. In the study this was done by submerging the sample in solutions of different pH and monitoring differences in fluorescence behavior. To this end, the technique was combined with balanced super-resolution optical fluctuation imaging (bSOFI) [146], which utilizes higher-order statistics to increase resolution and image contrast—provided that the emitters display uncorrelated, stochastic fluctuations.

Almost at the same time, this SMLM technique developed for monolayer hBN was successfully implemented to investigate the optical properties of hBN nanoparticles as small as (3.0 ± 0.7) nm, produced by cryogenic exfoliation (**Figure 2C**) [87]. The merit of the work was to demonstrate that hBN nanoparticles/nanoflakes possess a combination of optical and size properties that make them desirable for (bio-)imaging and sensing applications, either via SMLM or RESOLFT microscopy.

In a follow-up study [65], this SMLM technique was further improved to include the ability to perform spectral analysis of the emitters and thus producing super-resolved images containing spatial, spectral and temporal dynamics of the emitters (**Figure 2D**). This was achieved by utilizing a calcium fluoride ($CaF_2$) filter in one of the detection paths (**Figure 2D**, left). This dispersive element allowed for the simultaneous correlation of spatial and spectral mapping of each emitter—showcased in the study by clearly distinguishing two families of hBN emitters one displaying photoluminescence at ~585 nm and the other at ~640 nm (**Figure 2D**, right panel).

A key feature of this multimodal SMLM method is the ability to correlate different characteristics and properties of the fluorophores, in time. For instance, the study shows the possibility to extract differences in blinking photo-kinetics for the two families of emitters and understand their physical origin (e.g., charge separation or ionization of the defects, as these follow different dynamics).

The versatility of this single-molecule localization microscopy technique was recently highlighted in a remarkable experiment that succeeded in imaging proton transfer phenomena in water, at an interface with single-charge resolution (**Figures 3A**,**B**) [142].

The basic SMLM scheme is analogous to the ones described above. Multilayer hBN flakes were irradiated in low-power oxygen plasma to create a high density of surface defects. These defects are hypothesized to be $V_B^-$ and show a considerably different fluorescence behavior when exposed to air or submerged in aqueous solutions of different pH. Monitoring the photoluminescence at ~2 eV (~620 nm) reveals that only a few emitters are luminescent in air (~0.3 per 2 × 2 μm$^2$ area), while many more are when the sample is submerged in slightly acidic solutions (~70 per 2 × 2 μm$^2$ area, in a 3.4 pH solution). The proposed explanation is that the $V_B^-$ defects are optically dark but become active (emitting photons at ~ 2 eV) as solvated protons $H^+$ compensate their charge through the reaction $V_B^- + H^+ \rightarrow V_BH$. The SMLM technique thus allows monitoring—with high resolution, and over time—the occurrence of this protonation reaction in solution, at each one of the hBN defect sites.

Notably, SMLM can capture the specific hopping of protons between adjacent sites as these sites undergo "dark/bright" switching events corresponding to their $V_B^-/V_BH$ states. In the study, trajectories of single protons moving from site to site over distances up to ~1 μm (imaging resolution ~5–40 nm) were monitored over time (~180 s). Different behaviors were observed, and it was possible to extract parameters such as diffusion coefficients and mean square displacement of the moving protons (**Figure 3B**). The study was able to clearly show—at the single-molecule scale—the mechanism of desorption-limited transport of protons occurring in water at a solid/water interface between adjacent surface defects. It also underscores how the interface provides a preferential pathway for charge migration, which is relevant for several fields ranging from cellular transport and signaling, to catalysis and membrane dynamics. The study is a remarkable demonstration of the interfacial transport of protons in relation to the surrounding bulk water—a mechanism which, up to now, has been beyond reach due to the inability to measure directly the motion of single protons in water, with high-enough resolution.

## Nonlinear Optical Microscopy

In the context of high-resolution imaging, nonlinear optical microscopy deserves a special mention as it has become a powerful tool not just for imaging but also for (2D) material characterization [147, 148]. Nonlinear microscopy relies on multi-photon excitation of the fluorophores via virtual states, which produces a set of inherent benefits compared to traditional single-photon excitation [149, 150]. These include better fluorophores-to-background contrast due to lower background autofluorescence [151], excitation through a favorable biological window (NIR wavelengths, 650–900 nm, characterized by lower absorption from hemoglobin and water) [152], as well as improved imaging resolution [153, 154].

Nonlinear optical excitation of single-photon emitters (SPEs) in hexagonal boron nitride has been demonstrated [143]. In the

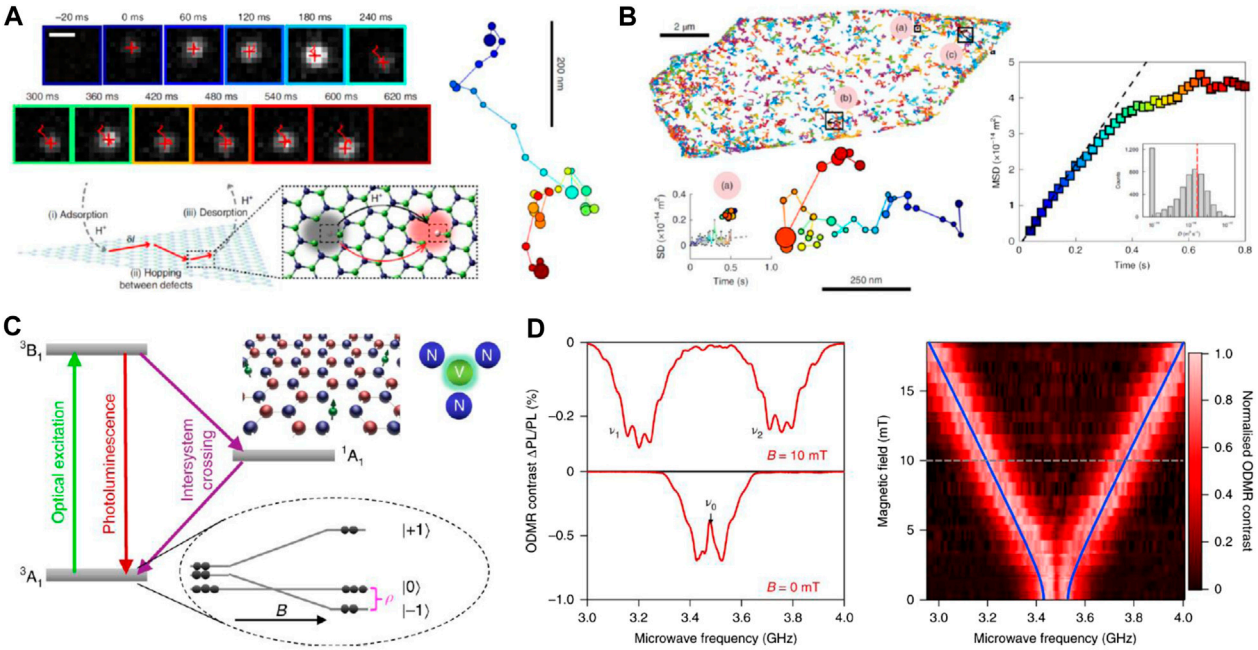


**FIGURE 3 |** Proton transport and quantum sensing in hBN. **(A)** Top left: time series for spatial migration of luminescence at the surface of the hBN flake, detected with wide-field SMLM (scale bar 500 nm; projected pixel size 100 nm). Right: Reconstructed trajectories showing successive activation of adjacent defects at the surface of the flake and color-coded with increasing time. Localized defects are represented as dots, with the radius corresponding to the localization uncertainty. Bottom left: schematic depicting luminescence migration events, consisting of successive proton adsorption, diffusion and proton desorption from the surface. **(B)** Top left: large-scale mapping of proton trajectories (200 ms) measured at the surface of the hBN flake. Bottom left: representative proton trajectory with the corresponding evolution of the square displacement (SD). Right: variation of the mean square displacement (MSD) as a function of time for the hBN flake. The dashed line is a linear fit from which the averaged diffusion coefficient is extracted $D = 2.8 \times 10^{-14}$ m$^2$ s$^{-1}$. Inset: distribution of the diffusion coefficient determined on individual trajectories, with the vertical dashed line being the average value. **(C)** Energy level scheme and atomic structure of the hBN $V_B^-$ center; note the triplet ground state of multiplicity $m_s = 0$ and $m_s = \pm 1$, with a magnetic field B lifting the $m_s = \pm 1$ degeneracy. **(D)** Optically detected magnetic resonance (ODMR) showing manipulation and read out of the spin state. The transitions $m_s = 0 \rightarrow +1$ and $m_s = 0 \rightarrow -1$ are shown by a drop in photoluminescence (ODMR contrast $\Delta PL/PL$) at the corresponding microwave resonant frequency. The dependence of the relative position between $m_s = 0$ and $m_s = \pm 1$ is the basis of quantum sensing applications based on reading out the spin state of the $V_B^-$ center. Figures adapted and reprinted with permission **(A,B)** [142] Copyright Springer Nature 2020 **(C,D)** [56] Copyright Springer Nature 2020.

study, individual atom-like defects with emission wavelength at 670 nm are excited either with a continuous laser at 532 nm or with a pulsed laser at 708 nm (pulses' duration 1 ps). The dependence of the SPEs' photon emission rate as a function of the excitation intensity reveals that excitation with the 708 nm pulsed laser takes place via a two-photon absorption process. In the experiment, large hBN flakes (size ~200 nm) were used, but the technique can be readily extended to smaller hBN nanoparticles (size <10 nm). The results thus demonstrate the possibility of employing nonlinear microscopy of fluorescent hBN nanoprobes as a feasible high-resolution imaging strategy, complementary to super-resolution microscopy.

## BEYOND OPTICAL IMAGING

Beyond SRM, hexagonal boron-nitride is showing promise as the hardware material for another class of high-resolution sensing applications at the nanoscale. These are based on monitoring the spin state of individual hBN quantum emitters in response to changes in the surrounding environment. In general, optically active quantum defects can be separated in two categories: single-photon emitters whose photoluminescence corresponds to transitions between well-defined quantum states, and so-called "spin centers" which exhibit coupling between the defects' intrinsic spin and their optical transitions. In other words, spin-centers display photoluminescence which is different depending on which spin state the emitter emits from. An archetype spin-center is the well-known nitrogen-vacancy ($NV^-$) center in diamond [155].

Spin-centers are sought after as potential qubits for solid-state, room-temperature quantum computation and information technologies [156], but also as ultra-sensitive nanoscale sensors [157]—which is of interest here. This is because their spin state can be manipulated and read out optically, while displaying extreme sensitivity to the local, surrounding environment.

The discovery of spin-centers in hBN is recent [56, 58], with the first identified one being the boron-vacancy center, $V_B^-$. The defect possesses distinguishable spin-optical transitions (**Figure 3C**). Specifically, the $V_B^-$ has a triplet ($S = 1$) ground state of multiplicity $m_s = 0$ and $m_s = \pm 1$, separated by a zero-field splitting (ZFS) energy $D_{gs} \cong 3.46$ GHz, in Planck's constant units $h$ (Note that, for completeness, the degeneracy

of the $m_s = \pm 1$ states is lifted due to the small off-axial component of the ZFS, $E_{gs} \cong 50$ MHz).

Optical excitation and cycling through the excited state of the defect 'spin-polarize' it in the $m_s = 0$ state, by preferentially populating it (**Figure 3C**). Applying a microwave field resonant with the transitions $m_s = 0 \leftrightarrow \pm 1$ allows manipulating the defect's spin state, which can then be read out, optically—as the excitation-decay cycle from the $m_s = 0$ ground state scatters more photons than the one from the $m_s = \pm 1$ one. These features are the basis of optically detected magnetic resonance (ODMR) in which the spin state of individual point-like defects can be prepared, manipulated, and read out optically at room temperature (**Figure 3D**).

This is relevant for high resolution, quantum sensing applications as the ground state ZFS splitting ($D_{gs}$, $E_{gs}$) can vary in response to external stimuli such as e.g., magnetic and electric fields, local chemistry or temperature. These quantities can therefore be measured directly using the $V_B^-$ defect in hBN as nanoprobes, simply by measuring changes in photoluminescence.

Spin defects in three-dimensional materials, such as diamond (e.g., nitrogen vacancy and silicon vacancy centers) [155, 158], silicon carbide (e.g., di-vacancy centers) [159, 160] and rare earth materials (e.g., Yb ions in yttrium orthovanadate hosts) [161, 162] have been extensively used for quantum sensing realizations. Examples include single-spin detection and magnetometry [163, 164], electrometry [165], decoherence microscopy [166], thermometry [167], optical trapping [168] and Forster resonance energy transfer [169, 170]. These exceptional demonstrations raise the question of how hBN $V_B^-$ centers benchmark in this context, especially since—currently—all the realizations involving hBN $V_B^-$ centers have been fundamental rather than practical.

There are several aspects that make spin-defects in hBN particularly attractive for quantum sensing applications. Unlike 3D semiconductor hosts, layered hBN are less prone to having unsaturated dangling bonds. These can act as fluctuating electron spins that generate magnetic noise and degrade the spin coherence—which is crucial for applications in quantum sensing [171].

The 2D nature of hBN confers it several additional, unique features. It allows for extremely high photon-extraction efficiencies. In fact, the out-coupling efficiency of hBN emitters is near-unity, as they are not surrounded by any high refractive index material and are not affected by Fresnel or total internal reflection, scattering and re-absorption [60]. This is desirable for nanoscale sensing applications based on photoluminescence detection, for it increases the signal-to-noise ratio and, thus, signal and/or temporal resolution.

Furthermore, the weak van der Waals forces between layers allow hBN to be readily transferred and integrated with other (hybrid) nanoscale systems made e.g., of 2D materials heterostructures [17, 172–174]. It also allows for the accurate placement of individual nanoprobe with respect to target areas or objects. This was demonstrated in a study that used a fluorescent hBN nanoparticle as an optical nanothermometer—placed deterministically onto a micro-circuit—to measure local temperature and potential hot spots in target areas of the device [175].

Another feature granted by the 2D nature of hBN is the potential close proximity between the emitter-sensors and the object or quantity to be sensed. This can be ~(sub)nm, which is highly desirable as, for instance in magnetometry, dipolar magnetic fields decay as the third inverse power of the distance between sensor and spin [176], which makes their relative separation a critical limiting factor for the sensitivity of the technique.

It should be noted that the field of spin-based quantum sensing, whilst well established in 3D semiconductors such as diamond, is at its absolute infancy in 2D hBN. The spin-addressable properties of the $V_B^-$ have been discovered only recently [56, 57]. In fact, while it has been shown that $V_B^-$ defects can be engineered in hBN via targeted irradiation, the isolation of individual defects is still beyond reach.

The research is certainly very active in the field. Shortly after the report of the $V_B^-$ center, a second and different type of spin-defect has been identified in hBN [58]. The defect is carbon-related (possibly the negatively charged $V_B C_N^-$). It emits with a sharp zero-phonon line wavelength at ~585 nm and is spin-active ($S \geq 1/2$) with a detectable ODMR spectrum. Again, the defect has not been isolated at a single-center level (ODMR has only been observed in ensemble, currently), but there is optimism as emission at ~585 nm from single centers is common in hBN.

## CONCLUSION AND OUTLOOK

Two-dimensional materials have garnered a lot of attention in recent years, mostly because their low dimensionality and relative ease of fabrication have allowed the accomplishment of a whole suite of interesting demonstrations difficult to attain with traditional 3D bulk materials. Amongst 2D materials, hexagonal boron-nitride has become object of intense research since 2015, when quantum (single-photon) emission from atom-like defects has been identified [52]. While hBN color centers have—arguably—been trailing behind their well-established counterparts in e.g., diamond and silicon carbide, they are quickly becoming an active field of research in their own right. Their characteristic optical (and recently discovered) spin properties combined with the unique physico-chemical features granted by the low dimensionality of the hBN host make them ideal systems for several fundamental and practical applications—including in high resolution imaging and sensing.

In this review, we have highlighted the role hBN quantum emitters have recently played in the realization of novel super-resolution imaging techniques (RESOLFT and SMLM), as well as their potential impact in advanced spin-based quantum sensing applications. Research geared towards exploiting hBN and its color centers for sensing and imaging is at its infancy. Future endeavors should focus on fully identifying the origin of the defects (besides the $V_B^-$) and improving material and color centers engineering to move from fundamental demonstrations to practical realizations. In this regard, experiments such as observing single proton transport at the solid/water interface

by hBN-based super-resolution microscopy are encouraging. They show that the material is offering novel capabilities that allow for the exploration of regimes inaccessible with alternative methods.

## AUTHOR CONTRIBUTIONS

The author confirms being the sole contributor of this work and has approved it for publication.

## REFERENCES


1. Sahl SJ, Hell SW, and Jakobs S Fluorescence nanoscopy in cell biology. *Nat Rev Mol Cel Biol* (2017) 18:685–701. doi:10.1038/nrm.2017.71
2. Hell SW Far-field optical nanoscopy. *Science* (2007) 316:1153–8. doi:10.1126/science.1137395
3. Balzarotti F, Eilers Y, Gwosch KC, Gynnå AH, Westphal V, Stefani FD, et al. Nanometer resolution imaging and tracking of fluorescent molecules with minimal photon fluxes. *Science* (2017) 355:606–12. doi:10.1126/science.aak9913
4. Vicidomini G, Bianchini P, and Diaspro A STED super-resolved microscopy. *Nat Methods* (2018) 15:173–82. doi:10.1038/nmeth.4593
5. Hell SW, and Kroug M Ground-state-depletion fluorscence microscopy: a concept for breaking the diffraction resolution limit. *Appl Phys B* (1995) 60: 495–7. doi:10.1007/bf01081333
6. Gustafsson MGL Surpassing the lateral resolution limit by a factor of two using structured illumination microscopy. SHORT COMMUNICATION. *J Microsc* (2000) 198:82–7. doi:10.1046/j.1365-2818.2000.00710.x
7. Gustafsson MGL Nonlinear structured-illumination microscopy: wide-field fluorescence imaging with theoretically unlimited resolution. *Proc Natl Acad Sci* (2005) 102:13081–6. doi:10.1073/pnas.0406877102
8. York AG, Chandris P, Nogare DD, Head J, Wawrzusin P, Fischer RS, et al. Instant super-resolution imaging in live cells and embryos via analog image processing. *Nat Methods* (2013) 10:1122–6. doi:10.1038/nmeth.2687
9. Rust MJ, Bates M, and Zhuang X Sub-diffraction-limit imaging by stochastic optical reconstruction microscopy (STORM). *Nat Methods* (2006) 3:793–6. doi:10.1038/nmeth929
10. Betzig E, Patterson GH, Sougrat R, Lindwasser OW, Olenych S, Bonifacino JS, et al. Imaging intracellular fluorescent proteins at nanometer resolution. *Science* (2006) 313:1642–5. doi:10.1126/science.1127344
11. Hess ST, Girirajan TPK, and Mason MD Ultra-high resolution imaging by fluorescence photoactivation localization microscopy. *Biophys J* (2006) 91: 4258–72. doi:10.1529/biophysj.106.091116
12. Sharonov A, and Hochstrasser RM Wide-field subdiffraction imaging by accumulated binding of diffusing probes. *Proc Natl Acad Sci* (2006) 103: 18911–6. doi:10.1073/pnas.0609643104
13. Gwosch KC, Pape JK, Balzarotti F, Hoess P, Ellenberg J, Ries J, et al. MINFLUX nanoscopy delivers 3D multicolor nanometer resolution in cells. *Nat Methods* (2020) 17:217–24. doi:10.1038/s41592-019-0688-0
14. Danzl JG, Sidenstein SC, Gregor C, Urban NT, Ilgen P, Jakobs S, et al. Coordinate-targeted fluorescence nanoscopy with multiple off states. *Nat Photon* (2016) 10:122–8. doi:10.1038/nphoton.2015.266
15. Göttfert F, Pleiner T, Heine J, Westphal V, Görlich D, Sahl SJ, et al. Strong signal increase in STED fluorescence microscopy by imaging regions of subdiffraction extent. *Proc Natl Acad Sci U S A* (2017) 114:2125–30. doi:10.1073/pnas.1621495114
16. Pujals S, Feiner-Gracia N, Delcanale P, Voets I, and Albertazzi L Super-resolution microscopy as a powerful tool to study complex synthetic materials. *Nat Rev Chem* (2019) 3:68–84. doi:10.1038/s41570-018-0070-2
17. Geim AK, and Grigorieva IV Van der Waals heterostructures. *Nature* (2013) 499:419–25. doi:10.1038/nature12385
18. Novoselov KS, Mishchenko A, Carvalho A, and Castro Neto AH 2D materials and van der Waals heterostructures. *Science* (2016) 353:aac9439. doi:10.1126/science.aac9439
19. Mak KF, and Shan J Opportunities and challenges of interlayer exciton control and manipulation. *Nat Nanotech* (2018) 13:974–6. doi:10.1038/s41565-018-0301-1
20. Jin C, Ma EY, Karni O, Regan EC, Wang F, and Heinz TF Ultrafast dynamics in van der Waals heterostructures. *Nat Nanotech* (2018) 13:994–1003. doi:10.1038/s41565-018-0298-5
21. Urbaszek B, and Srivastava A Materials in flatland twist and shine, *Nature* (2019) 567:39–40. doi:10.1038/d41586-019-00704-x
22. Qian X, Liu J, Fu L, and Li J Quantum spin Hall effect in two-dimensional transition metal dichalcogenides. *Science* (2014) 346:1344–7. doi:10.1126/science.1256815
23. Ceballos F, Bellus MZ, Chiu H-Y, and Zhao H Ultrafast charge separation and indirect exciton formation in a MoS2-MoSe2 van der Waals heterostructure. *ACS nano* (2014) 8:12717–24. doi:10.1021/nn505736z
24. Gong Y, Lin J, Wang X, Shi G, Lei S, Lin Z, et al. Vertical and in-plane heterostructures from WS2/MoS2 monolayers. *Nat Mater* (2014) 13: 1135–42. doi:10.1038/nmat4091
25. Rivera P, Seyler KL, Yu H, Schaibley JR, Yan J, Mandrus DG, et al. Valley-polarized exciton dynamics in a 2D semiconductor heterostructure. *Science* (2016) 351:688–91. doi:10.1126/science.aac7820
26. Rivera P, Yu H, Seyler KL, Wilson NP, Yao W, and Xu X Interlayer valley excitons in heterobilayers of transition metal dichalcogenides. *Nat Nanotech* (2018) 13:1004–15. doi:10.1038/s41565-018-0193-0
27 Hsu W.-T., Lin B.-H., Lu L.-S., Lee M.-H., Chu M.-W., Li L.-J., et al. Tailoring excitonic states of van der Waals bilayers through stacking configuration, band alignment, and valley spin. *Sci Adv* (2019) 5:eaax7407. doi:10.1126/sciadv.aax7407
28. Liu Y, Rang H, Rasmita A, Zhou Y, Li J, Xiong Q, et al. Room temperature nanocavity laser with interlayer excitons in 2D heterostructures. *Sci Adv* (2019) 5:eaav4506. doi:10.1126/sciadv.aav4506
29. Withers F, Del Pozo-Zamudio O, Mishchenko A, Rooney AP, Gholinia A, Watanabe K, et al. Light-emitting diodes by band-structure engineering in van der Waals heterostructures. *Nat Mater* (2015) 14:301–6. doi:10.1038/nmat4205
30. Gong C, Zhang H, Wang W, Colombo L, Wallace RM, and Cho K, Band alignment of two-dimensional transition metal dichalcogenides: application in tunnel field effect transistors. *Appl Phys Lett* (2013) 103:053513. doi:10.1063/1.4817409
31. Georgiou T, Jalil R, Belle BD, Britnell L, Gorbachev RV, Morozov SV, et al. Vertical field-effect transistor based on graphene-WS2 heterostructures for flexible and transparent electronics. *Nat Nanotech* (2013) 8:100. doi:10.1038/nnano.2012.224
32. Britnell L, Gorbachev RV, Jalil R, Belle BD, Schedin F, Mishchenko A, et al. Field-effect tunneling transistor based on vertical graphene heterostructures. *Science* (2012) 335:947–50. doi:10.1126/science.1218461
33. Aftab S, and Eom J Van der Waals 2D layered-material bipolar transistor. *2D Mater* (2019) 6:035005. doi:10.1088/2053-1583/ab1df2
34. Vu QA, Lee JH, Nguyen VL, Shin YS, Lim SC, Lee K, et al. Tuning carrier tunneling in van der Waals heterostructures for ultrahigh detectivity. *Nano Lett* (2017) 17:453–9. doi:10.1021/acs.nanolett.6b04449
35. Zhou X, Hu X, Zhou S, Song H, Zhang Q, Pi L, et al. Tunneling diode based on WSe2/SnS2 heterostructure incorporating high detectivity and responsivity. *Adv Mater* (2018) 30:1703286. doi:10.1002/adma.201703286
36. Meng J-H, Liu X, Zhang X-W, Zhang Y, Wang H-L, Yin Z-G, et al. Interface engineering for highly efficient graphene-on-silicon Schottky junction solar cells by introducing a hexagonal boron nitride interlayer. *Nano Energy* (2016) 28:44–50. doi:10.1016/j.nanoen.2016.08.028
37. Wang D, Lu Y, Meng J, Zhang X, Yin Z, Gao M, et al. Remote heteroepitaxy of atomic layered hafnium disulfide on sapphire through hexagonal boron nitride. *Nanoscale* (2019) 11:9310–8. doi:10.1039/c9nr01700c
38. Li X, Lin S, Lin X, Xu Z, Wang P, Zhang S, et al. Graphene/h-BN/GaAs sandwich diode as solar cell and photodetector. *Opt Express* (2016) 24: 134–45. doi:10.1364/oe.24.000134
39. Radisavljevic B, Whitwick MB, and Kis A Small-signal amplifier based on single-layer MoS2. *Appl Phys Lett* (2012) 101:043103. doi:10.1063/1.4738986
40. Alem N, Erni R, Kisielowski C, Rossell MD, Gannett W, and Zettl A Atomically thin hexagonal boron nitride probed by ultrahigh-resolution

transmission electron microscopy. *Phys Rev B* (2009) 80:155425. doi:10.1103/PhysRevB.80.155425
41. Elias C, Valvin P, Pelini T, Summerfield A, Mellor CJ, Cheng TS, et al. Direct band-gap crossover in epitaxial monolayer boron nitride. *Nat Commun* (2019) 10:2639. doi:10.1038/s41467-019-10610-5
42. Castelletto S, Inam FA, Sato S-i., and Boretti A Hexagonal boron nitride: a review of the emerging material platform for single-photon sources and the spin-photon interface. *Beilstein J Nanotechnol* (2020) 11:740–69. doi:10.3762/bjnano.11.61
43. Jobst J, van der Torren AJH, Krasovskii EE, Balgley J, Dean CR, Tromp RM, et al. Quantifying electronic band interactions in van der Waals materials using angle-resolved reflected-electron spectroscopy. *Nat Commun* (2016) 7:13621. doi:10.1038/ncomms13621
44. Sponza L, Amara H, Attaccalite C, Latil S, Galvani T, Paleari F, et al. Direct and indirect excitons in boron nitride polymorphs: a story of atomic configuration and electronic correlation. *Phys Rev B* (2018) 98:125206. doi:10.1103/PhysRevB.98.125206
45. Pakdel A, Bando Y, and Golberg D Nano boron nitride flatland. *Chem Soc Rev* (2014) 43:934–59. doi:10.1039/C3CS60260E
46. Kubota Y, Watanabe K, Tsuda O, and Taniguchi T Deep ultraviolet light-emitting hexagonal boron nitride synthesized at atmospheric pressure. *Science* (2007) 317:932–4. doi:10.1126/science.1144216
47. Alem N, Ramasse QM, Seabourne CR, Yazyev OV, Erickson K, Sarahan MC, et al. Subangstrom edge relaxations probed by electron microscopy in hexagonal boron nitride. *Phys Rev Lett* (2012) 109:205502. doi:10.1103/PhysRevLett.109.205502
48. Gibb AL, Alem N, Chen J-H, Erickson KJ, Ciston J, Gautam A, et al. Atomic resolution imaging of grain boundary defects in monolayer chemical vapor deposition-grown hexagonal boron nitride. *J Am Chem Soc* (2013) 135:6758–61. doi:10.1021/ja400637n
49. Zhu W, Wu Z, Foo GS, Gao X, Zhou M, Liu B, et al. Taming interfacial electronic properties of platinum nanoparticles on vacancy-abundant boron nitride nanosheets for enhanced catalysis. *Nat Commun* (2017) 8:15291. doi:10.1038/ncomms15291
50. Cretu O, Lin Y-C, and Suenaga K Evidence for active atomic defects in monolayer hexagonal boron nitride: a new mechanism of plasticity in two-dimensional materials. *Nano Lett* (2014) 14:1064–8. doi:10.1021/nl404735w
51. Sajid A, Reimers JR, and Ford MJ Defect states in hexagonal boron nitride: assignments of observed properties and prediction of properties relevant to quantum computation. *Phys Rev B* (2018) 97:064101. doi:10.1103/PhysRevB.97.064101
52. Tran TT, Bray K, Ford MJ, Toth M, and Aharonovich I Quantum emission from hexagonal boron nitride monolayers. *Nat Nanotech* (2016) 11:37–41. doi:10.1038/nnano.2015.242
53. Abdi M, Chou J-P, Gali A, and Plenio MB Color centers in hexagonal boron nitride monolayers: a group theory and ab initio analysis. *ACS Photon* (2018) 5:1967–76. doi:10.1021/acsphotonics.7b01442
54. Tran TT, Elbadawi C, Totonjian D, Lobo CJ, Grosso G, Moon H, et al. Robust multicolor single photon emission from point defects in hexagonal boron nitride. *ACS Nano* (2016) 10:7331–8. doi:10.1021/acsnano.6b03602
55. Shotan Z, Jayakumar H, Considine CR, Mackoit M, Fedder H, Wrachtrup J, et al. Photoinduced modification of single-photon emitters in hexagonal boron nitride. *ACS Photon* (2016) 3:2490–6. doi:10.1021/acsphotonics.6b00736
56. Gottscholl A, Kianinia M, Soltamov V, Orlinskii S, Mamin G, Bradac C, et al. Initialization and read-out of intrinsic spin defects in a van der Waals crystal at room temperature. *Nat Mater* (2020) 19:540. doi:10.1038/s41563-020-0619-6
57. Ivády V, Barcza G, Thiering G, Li S, Hamdi H, Chou J-P, et al. Ab initio theory of the negatively charged boron vacancy qubit in hexagonal boron nitride. *Npj Comput Mater* (2020) 6:41. doi:10.1038/s41524-020-0305-x
58. Mendelson N, Chugh D, Reimers JR, Cheng TS, Gottscholl A, Long H, et al. Identifying carbon as the source of visible single-photon emission from hexagonal boron nitride. *Nat Mater* (2020). doi:10.1038/s41563-020-00850-y
59. Kianinia M, Regan B, Tawfik SA, Tran TT, Ford MJ, Aharonovich I, et al. Robust solid-state quantum system operating at 800 K. *ACS Photon* (2017) 4:768–73. doi:10.1021/acsphotonics.7b00086
60. Vogl T, Campbell G, Buchler BC, Lu Y, and Lam PK Fabrication and deterministic transfer of high-quality quantum emitters in hexagonal boron nitride. *ACS Photon* (2018) 5:2305–12. doi:10.1021/acsphotonics.8b00127
61. Exarhos AL, Hopper DA, Patel RN, Doherty MW, and Bassett LC Magnetic-field-dependent quantum emission in hexagonal boron nitride at room temperature. *Nat Commun* (2019) 10:222. doi:10.1038/s41467-018-08185-8
62. Xia Y, Li Q, Kim J, Bao W, Gong C, Yang S, et al. Room-temperature giant Stark effect of single photon emitter in van der Waals material. *Nano Lett* (2019) 19:7100–5. doi:10.1021/acs.nanolett.9b02640
63. Nikolay N, Mendelson N, Sadzak N, Böhm F, Tran TT, Sontheimer B, et al. Very large and reversible Stark-shift tuning of single emitters in layered hexagonal boron nitride. *Phys Rev Appl* (2019) 11:041001. doi:10.1103/PhysRevApplied.11.041001
64. Kianinia M, Bradac C, Sontheimer B, Wang F, Tran TT, Nguyen M, et al. All-optical control and super-resolution imaging of quantum emitters in layered materials. *Nat Commun* (2018) 9:874. doi:10.1038/s41467-018-03290-0
65. Comtet J, Glushkov E, Navikas V, Feng J, Babenko V, Hofmann S, et al. Wide-field spectral super-resolution mapping of optically active defects in hexagonal boron nitride. *Nano Lett* (2019) 19:2516–23. doi:10.1021/acs.nanolett.9b00178
66. Shi Y, Hamsen C, Jia X, Kim KK, Reina A, Hofmann M, et al. Synthesis of few-layer hexagonal boron nitride thin film by chemical vapor deposition. *Nano Lett* (2010) 10:4134–9. doi:10.1021/nl1023707
67. Song L, Ci L, Lu H, Sorokin PB, Jin C, Ni J, et al. Large scale growth and characterization of atomic hexagonal boron nitride layers. *Nano Lett* (2010) 10:3209–15. doi:10.1021/nl1022139
68. Yu J, Qin L, Hao Y, Kuang S, Bai X, Chong Y-M, et al. Vertcally aligned boron nitride nanosheets: chemical vapor synthesis, ultraviolet light emission, and superhydrophobicity. *ACS Nano* (2010) 4:414–22. doi:10.1021/nn901204c
69. Xu M, Fujita D, Chen H, and Hanagata N Formation of monolayer and few-layer hexagonal boron nitride nanosheets via surface segregation. *Nanoscale* (2011) 3:2854–8. doi:10.1039/C1NR10294J
70. Lian G, Zhang X, Tan M, Zhang S, Cui D, and Wang Q Facile synthesis of 3D boron nitride nanoflowers composed of vertically aligned nanoflakes and fabrication of graphene-like BN by exfoliation. *J Mater Chem* (2011) 21:9201–7. doi:10.1039/C0JM04503A
71. Han W-Q, Yu H-G, and Liu Z Convert graphene sheets to boron nitride and boron nitride-carbon sheets via a carbon-substitution reaction. *Appl Phys Lett* (2011) 98:203112. doi:10.1063/1.3593492
72. Novoselov KS, Jiang D, Schedin F, Booth TJ, Khotkevich VV, Morozov SV, et al. Two-dimensional atomic crystals. *Proc Natl Acad Sci* (2005) 102:10451–3. doi:10.1073/pnas.0502848102
73. Li LH, Chen Y, Behan G, Zhang H, Petravic M, and Glushenkov AM Large-scale mechanical peeling of boron nitride nanosheets by low-energy ball milling. *J Mater Chem* (2011) 21:11862–6. doi:10.1039/C1JM11192B
74. Pacilé D, Meyer JC, Girit ÇÖ, and Zettl A The two-dimensional phase of boron nitride: few-atomic-layer sheets and suspended membranes. *Appl Phys Lett* (2008) 92:133107. doi:10.1063/1.2903702
75. Liu L, Xiong Z, Hu D, Wu G, Liu B, and Chen P Solid exfoliation of hexagonal boron nitride crystals for the synthesis of few-layer boron nitride nanosheets. *Chem Lett* (2013) 42:1415–6. doi:10.1246/cl.130562
76. Han W-Q, Wu L, Zhu Y, Watanabe K, and Taniguchi T Structure of chemically derived mono- and few-atomic-layer boron nitride sheets. *Appl Phys Lett* (2008) 93:223103. doi:10.1063/1.3041639
77. Warner JH, Rümmeli MH, Bachmatiuk A, and Büchner B Atomic resolution imaging and topography of boron nitride sheets produced by chemical exfoliation. *ACS Nano* (2010) 4:1299–304. doi:10.1021/nn901648q
78. Li X, Hao X, Zhao M, Wu Y, Yang J, Tian Y, et al. Exfoliation of hexagonal boron nitride by molten hydroxides. *Adv Mater* (2013) 25:2200–4. doi:10.1002/adma.201204031
79. Chen X, Dobson JF, and Raston CL Vortex fluidic exfoliation of graphite and boron nitride. *Chem Commun* (2012) 48:3703–5. doi:10.1039/C2CC17611D
80. Meyer JC, Chuvilin A, Algara-Siller G, Biskupek J, and Kaiser U Selective sputtering and atomic resolution imaging of atomically thin boron nitride membranes. *Nano Lett* (2009) 9:2683–9. doi:10.1021/nl9011497

81. Jin C, Lin F, Suenaga K, and Iijima S Fabrication of a freestanding boron nitride single layer and its defect assignments. *Phys Rev Lett* (2009) 102: 195505. doi:10.1103/PhysRevLett.102.195505
82. Jiang X-F, Weng Q, Wang X-B, Li X, Zhang J, Golberg D, et al. Recent progress on fabrications and applications of boron nitride nanomaterials: a review. *J Mat Sci Technol* (2015) 31:589–98. doi:10.1016/j.jmst.2014.12.008
83. Emanet M, Sen Ö, Taşkin IÇ, and Çulha M Synthesis, functionalization, and bioapplications of two-dimensional boron nitride nanomaterials. *Front Bioeng Biotechnol* (2019) 7:363. doi:10.3389/fbioe.2019.00363
84. DeepikaLi LH, Glushenkov AM, Hait SK, Hodgson P, and Chen Y High-efficient production of boron nitride nanosheets via an optimized ball milling process for lubrication in oil. *Sci Rep* (2014) 4:7288. doi:10.1038/srep07288
85. Bari R, Parviz D, Khabaz F, Klaassen CD, Metzler SD, Hansen MJ, et al. Liquid phase exfoliation and crumpling of inorganic nanosheets. *Phys Chem Chem Phys* (2015) 17:9383–93. doi:10.1039/C5CP00294J
86. Smith RJ, King PJ, Lotya M, Wirtz C, Khan U, De S, et al. Large-scale exfoliation of inorganic layered compounds in aqueous surfactant solutions. *Adv Mater* (2011) 23:3944–8. doi:10.1002/adma.201102584
87. Duong NMH, Glushkov E, Chernev A, Navikas V, Comtet J, Nguyen MAP, et al. Facile production of hexagonal boron nitride nanoparticles by cryogenic exfoliation. *Nano Lett* (2019) 19:5417–22. doi:10.1021/acs.nanolett.9b01913
88. Wang Y, Liu Y, Zhang J, Wu J, Xu H, Wen X, et al. Cryo-mediated exfoliation and fracturing of layered materials into 2D quantum dots. *Sci Adv* (2017) 3: e1701500. doi:10.1126/sciadv.1701500
89. Huo B, Liu B, Chen T, Cui L, Xu G, Liu M, et al. One-step synthesis of fluorescent boron nitride quantum dots via a hydrothermal strategy using melamine as nitrogen source for the detection of ferric ions. *Langmuir* (2017) 33:10673–8. doi:10.1021/acs.langmuir.7b01699
90. Bradac C, Gaebel T, Naidoo N, Rabeau JR, and Barnard AS Prediction and measurement of the size-dependent stability of fluorescence in diamond over the entire nanoscale. *Nano Lett* (2009) 9:3555–64. doi:10.1021/nl9017379
91. Bradac C, Gaebel T, Naidoo N, Sellars MJ, Twamley J, Brown LJ, et al. Observation and control of blinking nitrogen-vacancy centres in discrete nanodiamonds. *Nat Nanotech* (2010) 5:345–9. doi:10.1038/nnano.2010.56
92. Nagl A, Hemelaar SR, and Schirhagl R Improving surface and defect center chemistry of fluorescent nanodiamonds for imaging purposes-a review. *Anal Bioanal Chem* (2015) 407:7521–36. doi:10.1007/s00216-015-8849-1
93. Noh G, Choi D, Kim J-H, Im D-G, Kim Y-H, Seo H, et al. Stark tuning of single-photon emitters in hexagonal boron nitride. *Nano Lett* (2018) 18: 4710–5. doi:10.1021/acs.nanolett.8b01030
94. Wang X, Ren X, Kahen K, Hahn MA, Rajeswaran M, Maccagnano-Zacher S, et al. Non-blinking semiconductor nanocrystals. *Nature* (2009) 459:686–9. doi:10.1038/nature08072
95. Bradac C, Gaebel T, Pakes CI, Say JM, Zvyagin AV, and Rabeau JR Effect of the nanodiamond host on a nitrogen-vacancy color-centre emission state. *Small* (2013) 9:132–9. doi:10.1002/smll.201200574
96. Fu K-MC, Santori C, Barclay PE, and Beausoleil RG Conversion of neutral nitrogen-vacancy centers to negatively charged nitrogen-vacancy centers through selective oxidation. *Appl Phys Lett* (2010) 96:121907. doi:10.1063/1.3364135
97. Rondin L, Dantelle G, Slablab A, Grosshans F, Treussart F, Bergonzo P, et al. Surface-induced charge state conversion of nitrogen-vacancy defects in nanodiamonds. *Phys Rev B* (2010) 82:115449. doi:10.1103/physrevb.82.115449
98. Salvetti A, Rossi L, Iacopetti P, Li X, Nitti S, Pellegrino T, et al. In vivobiocompatibility of boron nitride nanotubes: effects on stem cell biology and tissue regeneration in planarians. *Nanomedicine* (2015) 10: 1911–22. doi:10.2217/nnm.15.46
99. Chen X, Wu P, Rousseas M, Okawa D, Gartner Z, Zettl A, et al. Boron nitride nanotubes are noncytotoxic and can be functionalized for interaction with proteins and cells. *J Am Chem Soc* (2009) 131:890–1. doi:10.1021/ja807334b
100. Kıvanç M, Barutca B, Koparal AT, Goncu Y, Boutanci SH, Ay N, et al. Effects of hexagonal boron nitride nanoparticles on antimicrobial and antibiofilm activities, cell viability. *Mater Sci Eng C* (2018) 91:115–24. doi:10.1016/j.msec.2018.05.028
101. Lu T, Wang L, Jiang Y, liu Q, and Huang C Hexagonal boron nitride nanoplates as emerging biological nanovectors and their potential applications in biomedicine. *J Mater Chem B* (2016) 4:6103–10. doi:10.1039/c6tb01481j
102. Lahiri D, Singh V, Benaduce AP, Seal S, Kos L, and Agarwal A Boron nitride nanotube reinforced hydroxyapatite composite: mechanical and tribological performance and *in-vitro* biocompatibility to osteoblasts. *J Mech Behav Biomed Mater* (2011) 4:44–56. doi:10.1016/j.jmbbm.2010.09.005
103. Liu L, Xiao L, Li M, Zhang X, Chang Y, Shang L, et al. Effect of hexagonal boron nitride on high-performance polyether ether ketone composites. *Colloid Polym Sci* (2016) 294:127–33. doi:10.1007/s00396-015-3733-2
104. Ciofani G Potential applications of boron nitride nanotubes as drug delivery systems. *Expert Opin Drug Deliv* (2010) 7:889–93. doi:10.1517/17425247.2010.499897
105. Ciofani G, Ricotti L, Danti S, Menciassi A, Chiellini F, D'Alessandro D, et al. Investigation of interactions between poly-L-lysine-coated boron nitride nanotubes and C2C12 cells: up-take, cytocompatibility, and differentiation. *Ijn* (2010) 5:285–95. doi:10.2147/ijn.s9879
106. Ciofani G, Raffa V, Menciassi A, and Cuschieri A Cytocompatibility, interactions, and uptake of polyethyleneimine-coated boron nitride nanotubes by living cells: confirmation of their potential for biomedical applications. *Biotechnol Bioeng* (2008) 101:850–8. doi:10.1002/bit.21952
107. Ciofani G, Raffa V, Menciassi A, and Cuschieri A Folate functionalized boron nitride nanotubes and their selective uptake by glioblastoma multiforme cells: implications for their use as boron carriers in clinical boron neutron capture therapy. *Nanoscale Res Lett* (2008) 4:113. doi:10.1007/s11671-008-9210-9
108. Horváth L, Magrez A, Golberg D, Zhi C, Bando Y, Smajda R, et al. *In vitro* investigation of the cellular toxicity of boron nitride nanotubes. *ACS Nano* (2011) 5:3800–10. doi:10.1021/nn200139h
109. Li X, Wang X, Zhang J, Hanagata N, Wang X, Weng Q, et al. Hollow boron nitride nanospheres as boron reservoir for prostate cancer treatment. *Nat Commun* (2017) 8:13936. doi:10.1038/ncomms13936
110. Ferreira TH, Silva PRO, Santos RG, and Sousa EMB (2011). A novel synthesis route to produce boron nitride nanotubes for bioapplications. *J Biomat Nanobiotechnol* 2, 426–34. doi:10.4236/jbnb.2011.24052
111. Weng Q, Wang X, Wang X, Bando Y, and Golberg D Functionalized hexagonal boron nitride nanomaterials: emerging properties and applications. *Chem Soc Rev* (2016) 45:3989–4012. doi:10.1039/C5CS00869G
112. Lu F, Wang F, Cao L, Kong CY, and Huang X Hexagonal boron nitride nanomaterials: advances towards bioapplications. *Nanosci Nanotechnol Lett* (2012) 4:949–61. doi:10.1166/nnl.2012.1444
113. Kalay S, Yilmaz Z, Sen O, Emanet M, Kazanc E, and Çulha M Synthesis of boron nitride nanotubes and their applications. *Beilstein J Nanotechnol* (2015) 6:84–102. doi:10.3762/bjnano.6.9
114. Gao Z, Zhi C, Bando Y, Golberg D, and Serizawa T Noncovalent functionalization of boron nitride nanotubes in aqueous media opens application roads in nanobiomedicine. *Nanobiomedicine* (2014) 1:7. doi:10.5772/60000
115. Weng Q, Wang B, Wang X, Hanagata N, Li X, Liu D, et al. Highly water-soluble, porous, and biocompatible boron nitrides for anticancer drug delivery. *ACS nano* (2014) 8:6123–30. doi:10.1021/nn5014808
116. Zhi CY, Bando Y, Terao T, Tang CC, Kuwahara H, and Golberg D Chemically activated boron nitride nanotubes. *Chem Asian J* (2009) 4:1536–40. doi:10.1002/asia.200900158
117. Lin Y, Williams TV, Xu T-B, Cao W, Elsayed-Ali HE, and Connell JW Aqueous dispersions of few-layered and monolayered hexagonal boron nitride nanosheets from sonication-assisted hydrolysis: critical role of water. *J Phys Chem C* (2011) 115:2679–85. doi:10.1021/jp110985w
118. Sainsbury T, Satti A, May P, Wang Z, McGovern I, Gun'ko YK, et al. Oxygen radical functionalization of boron nitride nanosheets. *J Am Chem Soc* (2012) 134:18758–71. doi:10.1021/ja3080665
119. Pakdel A, Bando Y, and Golberg D Plasma-assisted interface engineering of boron nitride nanostructure films. *ACS Nano* (2014) 8:10631–9. doi:10.1021/nn5041729
120. Lee D, Lee B, Park KH, Ryu HJ, Jeon S, and Hong SH Scalable exfoliation process for highly soluble boron nitride nanoplatelets by hydroxide-assisted ball milling. *Nano Lett* (2015) 15:1238–44. doi:10.1021/nl504397h
121. Weng Q, Ide Y, Wang X, Wang X, Zhang C, Jiang X, et al. Design of BN porous sheets with richly exposed (002) plane edges and their application as

TiO2 visible light sensitizer. *Nano Energy* (2015) 16:19–27. doi:10.1016/j.nanoen.2015.06.004
122. Xie S-Y, Wang W, Fernando KAS, Wang X, Lin Y, and Sun Y-P Solubilization of boron nitride nanotubes. *Chem Commun* (2005) 3670–2. doi:10.1039/B505330G
123. Lin Y, Williams TV, and Connell JW Soluble, exfoliated hexagonal boron nitride nanosheets. *J Phys Chem Lett* (2010) 1:277–83. doi:10.1021/jz9002108
124. Ikuno T, Sainsbury T, Okawa D, Fréchet JMJ, and Zettl A Amine-functionalized boron nitride nanotubes. *Solid State Commun* (2007) 142:643–6. doi:10.1016/j.ssc.2007.04.010
125. Liao Y, Chen Z, Connell JW, Fay CC, Park C, Kim J-W, et al. Chemical sharpening, shortening, and unzipping of boron nitride nanotubes. *Adv Funct Mater* (2014) 24:4497–506. doi:10.1002/adfm.201400599
126. Kim D, Nakajima S, Sawada T, Iwasaki M, Kawauchi S, Zhi C, et al. Sonication-assisted alcoholysis of boron nitride nanotubes for their sidewalls chemical peeling. *Chem Commun* (2015) 51:7104–7. doi:10.1039/C5CC00388A
127. Sainsbury T, O'Neill A, Passarelli MK, Seraffon M, Gohil D, Gnaniah S, et al. Dibromocarbene functionalization of boron nitride nanosheets: toward band gap manipulation and nanocomposite applications. *Chem Mater* (2014) 26:7039–50. doi:10.1021/cm503475t
128. Shin H, Guan J, Zgierski MZ, Kim KS, Kingston CT, and Simard B Covalent functionalization of boron nitride nanotubes via reduction chemistry. *ACS Nano* (2015) 9:12573–82. doi:10.1021/acsnano.5b06523
129. Golberg D, Bando Y, Tang CC, and Zhi CY Boron nitride nanotubes. *Adv Mater* (2007) 19:2413–32. doi:10.1002/adma.200700179
130. Zhi C, Bando Y, Tang C, Honda S, Sato K, Kuwahara H, et al. Covalent functionalization: towards soluble multiwalled boron nitride nanotubes. *Angew Chem Int Ed* (2005) 44:7932–5. doi:10.1002/anie.200502846
131. Huang X, Zhi C, Jiang P, Golberg D, Bando Y, and Tanaka T Polyhedral oligosilsesquioxane-modified boron nitride nanotube based epoxy nanocomposites: an ideal dielectric material with high thermal conductivity. *Adv Funct Mater* (2013) 23:1824–31. doi:10.1002/adfm.201201824
132. Ciofani G, Genchi GG, Liakos I, Athanassiou A, Dinucci D, Chiellini F, et al. A simple approach to covalent functionalization of boron nitride nanotubes. *J Colloid Interf Sci* (2012) 374:308–14. doi:10.1016/j.jcis.2012.01.049
133. Bhattacharya A, Bhattacharya S, and Das GP Band gap engineering by functionalization of BN sheet. *Phys Rev B* (2012) 85:035415. doi:10.1103/PhysRevB.85.035415
134. Li X, Zhao J, and Yang J Semihydrogenated BN sheet: a promising visible-light driven photocatalyst for water splitting. *Sci Rep* (2013) 3:1858. doi:10.1038/srep01858
135. Tang C, Bando Y, Huang Y, Yue S, Gu C, Xu F, et al. Fluorination and electrical conductivity of BN nanotubes. *J Am Chem Soc* (2005) 127:6552–3. doi:10.1021/ja042388u
136. Wolters J, Sadzak N, Schell AW, Schröder T, and Benson O Measurement of the ultrafast spectral diffusion of the optical transition of nitrogen vacancy centers in nano-size diamond using correlation interferometry. *Phys Rev Lett* (2013) 110:027401. doi:10.1103/PhysRevLett.110.027401
137. Neuhauser RG, Shimizu KT, Woo WK, Empedocles SA, and Bawendi MG Correlation between fluorescence intermittency and spectral diffusion in single semiconductor quantum dots. *Phys Rev Lett* (2000) 85:3301–4. doi:10.1103/PhysRevLett.85.3301
138. Kobayashi Y, Inose H, Nakagawa T, Gonda K, Takeda M, Ohuchi N, et al. Control of shell thickness in silica-coating of Au nanoparticles and their X-ray imaging properties. *J Colloid Interf Sci* (2011) 358:329–33. doi:10.1016/j.jcis.2011.01.058
139. Deng W, Jin D, Drozdowicz-Tomsia K, Yuan J, Wu J, and Goldys EM Ultrabright Eu-doped plasmonic Ag@SiO2 nanostructures: time-gated bioprobes with single particle sensitivity and negligible background. *Adv Mater* (2011) 23:4649–54. doi:10.1002/adma.201102027
140. Abidi IH, Mendelson N, Tran TT, Tyagi A, Zhuang M, Weng LT, et al. Selective defect formation in hexagonal boron nitride. *Adv Opt Mater* (2019) 7:1900397. doi:10.1002/adom.201900397
141. Feng J, Deschout H, Caneva S, Hofmann S, Lončarić I, Lazić P, et al. Imaging of optically active defects with nanometer resolution. *Nano Lett* (2018) 18:1739–44. doi:10.1021/acs.nanolett.7b04819
142. Comtet J, Grosjean B, Glushkov E, Avsar A, Watanabe K, Taniguchi T, et al. Direct observation of water-mediated single-proton transport between hBN surface defects. *Nat Nanotechnol* (2020) 15:598–604. doi:10.1038/s41565-020-0695-4
143. Schell AW, Tran TT, Takashima H, Takeuchi S, and Aharonovich I Non-linear excitation of quantum emitters in hexagonal boron nitride multiplayers. *APL Photon* (2016) 1:091302. doi:10.1063/1.4961684
144. Sontheimer B, Braun M, Nikolay N, Sadzak N, Aharonovich I, and Benson O Photodynamics of quantum emitters in hexagonal boron nitride revealed by low-temperature spectroscopy. *Phys Rev B* (2017) 96:121202. doi:10.1103/PhysRevB.96.121202
145. Tran TT, Bradac C, Solntsev AS, Toth M, and Aharonovich I Suppression of spectral diffusion by anti-Stokes excitation of quantum emitters in hexagonal boron nitride. *Appl Phys Lett* (2019) 115:071102. doi:10.1063/1.5099631
146. Dertinger T, Colyer R, Iyer G, Weiss S, and Enderlein J Fast, background-free, 3D super-resolution optical fluctuation imaging (SOFI). *Proc Natl Acad Sci U S A* (2009) 106:22287–92. doi:10.1073/pnas.0907866106
147. Wen X, Gong Z, and Li D Nonlinear optics of two-dimensional transition metal dichalcogenides. *InfoMat* (2019) 1:317–37. doi:10.1002/inf2.12024
148. Zhou L, Fu H, Lv T, Wang C, Gao H, Li D, et al. Nonlinear optical characterization of 2D materials. *Nanomaterials* (2020) 10:2263. doi:10.3390/nano10112263
149. Kaiser W, and Garrett CGB Two-photon excitation in CaF2:Eu2+. *Phys Rev Lett* (1961) 7:229–31. doi:10.1103/PhysRevLett.7.229
150. Friedrich DM Two-photon molecular spectroscopy. *J Chem Educ* (1982) 59:472. doi:10.1021/ed059p472
151. Denk W, Strickler J, and Webb W Two-photon laser scanning fluorescence microscopy. *Science* (1990) 248:73–6. doi:10.1126/science.2321027
152. Weissleder R A clearer vision for *in vivo* imaging. *Nat Biotechnol* (2001) 19:316–7. doi:10.1038/86684
153. Doi A, Oketani R, Nawa Y, and Fujita K High-resolution imaging in two-photon excitation microscopy using *in situ* estimations of the point spread function. *Biomed Opt Express* (2018) 9:202–13. doi:10.1364/BOE.9.000202
154. Zhilie T, Chuping Y, Hongjin P, Ruisheng L, and Songhao L Imaging theory and resolution improvement of two-photon confocal microscopy. *Sci China Ser A-Math* (2002) 45:1468–78. doi:10.1007/BF02880042
155. Doherty MW, Manson NB, Delaney P, Jelezko F, Wrachtrup J, and Hollenberg LCL The nitrogen-vacancy colour centre in diamond. *Phys Rep* (2013) 528:1–45. doi:10.1016/j.physrep.2013.02.001
156. Childress L, and Hanson R Diamond NV centers for quantum computing and quantum networks. *MRS Bull* (2013) 38:134–8. doi:10.1557/mrs.2013.20
157. Degen CL, Reinhard F, and Cappellaro P Quantum sensing. *Rev Mod Phys* (2017) 89:035002. doi:10.1103/RevModPhys.89.035002
158. Bradac C, Gao W, Forneris J, Trusheim ME, and Aharonovich I Quantum nanophotonics with group IV defects in diamond. *Nat Commun* (2019) 10:5625. doi:10.1038/s41467-019-13332-w
159. Nagy R, Niethammer M, Widmann M, Chen Y-C, Udvarhelyi P, Bonato C, et al. High-fidelity spin and optical control of single silicon-vacancy centres in silicon carbide. *Nat Commun* (2019) 10:1954. doi:10.1038/s41467-019-09873-9
160. Castelletto S, Johnson BC, Ivády V, Stavrias N, Umeda T, Gali A, et al. A silicon carbide room-temperature single-photon source. *Nat Mater* (2014) 13:151–6. doi:10.1038/nmat3806
161. Zhong M, Hedges MP, Ahlefeldt RL, Bartholomew JG, Beavan SE, Wittig SM, et al. Optically addressable nuclear spins in a solid with a six-hour coherence time. *Nature* (2015) 517:177–80. doi:10.1038/nature14025
162. Kindem JM, Ruskuc A, Bartholomew JG, Rochman J, Huan YQ, and Faraon A Control and single-shot readout of an ion embedded in a nanophotonic cavity. *Nature* (2020) 580:201–4. doi:10.1038/s41586-020-2160-9
163. Grinolds MS, Hong S, Maletinsky P, Luan L, Lukin MD, Walsworth RL, et al. Nanoscale magnetic imaging of a single electron spin under ambient conditions. *Nat Phys* (2013) 9:215–9. doi:10.1038/nphys2543
164. Grinolds MS, Warner M, De Greve K, Dovzhenko Y, Thiel L, Walsworth RL, et al. Subnanometre resolution in three-dimensional magnetic resonance imaging of individual dark spins. *Nat Nanotech* (2014) 9:279–84. doi:10.1038/nnano.2014.30

165. Dolde F, Fedder H, Doherty MW, Nöbauer T, Rempp F, Balasubramanian G, et al. Electric-field sensing using single diamond spins. *Nat Phys* (2011) 7: 459–63. doi:10.1038/nphys1969
166. Cole JH, and Hollenberg LCL Scanning quantum decoherence microscopy. *Nanotechnology* (2009) 20:495401. doi:10.1088/0957-4484/20/49/495401
167. Kucsko G, Maurer PC, Yao NY, Kubo M, Noh HJ, Lo PK, et al. Nanometre-scale thermometry in a living cell. *Nature* (2013) 500:54–8. doi:10.1038/nature12373
168. Geiselmann M, Juan ML, Renger J, Say JM, Brown LJ, de Abajo FJG, et al. Three-dimensional optical manipulation of a single electron spin. *Nat Nanotech* (2013) 8:175–9. doi:10.1038/nnano.2012.259
169. Chen Y-Y, Shu H, Kuo Y, Tzeng Y-K, and Chang H-C Measuring Förster resonance energy transfer between fluorescent nanodiamonds and near-infrared dyes by acceptor photobleaching. *Diamond Relat Mater* (2011) 20:803–7. doi:10.1016/j.diamond.2011.03.039
170. Tisler J, Reuter R, Lämmle A, Jelezko F, Balasubramanian G, Hemmer PR, et al. Highly efficient FRET from a single nitrogen-vacancy center in nanodiamonds to a single organic molecule. *ACS Nano* (2011) 5:7893–8. doi:10.1021/nn2021259
171. Herbschleb ED, Kato H, Maruyama Y, Danjo T, Makino T, Yamasaki S, et al. Ultra-long coherence times amongst room-temperature solid-state spins. *Nat Commun* (2019) 10:3766. doi:10.1038/s41467-019-11776-8
172. Liu Y, Zhang S, He J, Wang ZM, and Liu Z Recent progress in the fabrication, properties, and devices of heterostructures based on 2D materials. *Nano-Micro Lett* (2019) 11:13. doi:10.1007/s40820-019-0245-5
173. Frisenda R, Navarro-Moratalla E, Gant P, Pérez De Lara D, Jarillo-Herrero P, Gorbachev RV, et al. Recent progress in the assembly of nanodevices and van der Waals heterostructures by deterministic placement of 2D materials. *Chem Soc Rev* (2018) 47:53–68. doi:10.1039/C7CS00556C
174. Kim K, Yankowitz M, Fallahazad B, Kang S, Movva HCP, Huang S, et al. van der Waals heterostructures with high accuracy rotational alignment. *Nano Lett* (2016) 16:1989–95. doi:10.1021/acs.nanolett.5b05263
175. Chen Y, Tran TN, Duong NMH, Li C, Toth M, Bradac C, et al. Optical thermometry with quantum emitters in hexagonal boron nitride. *ACS Appl Mater Inter* (2020) 12:25464–70. doi:10.1021/acsami.0c05735
176. Rondin L, Tetienne J-P, Hingant T, Roch J-F, Maletinsky P, and Jacques V Magnetometry with nitrogen-vacancy defects in diamond. *Rep Prog Phys* (2014) 77:056503. doi:10.1088/0034-4885/77/5/056503

**Conflict of Interest:** The author declares that the research was conducted in the absence of any commercial or financial relationships that could be construed as a potential conflict of interest.